Planetary and Space Science 228 (2023) 105651

Contents lists available at ScienceDirect

Planetary and Space Science

journal homepage: www.elsevier.com/locate/pss

Experimental investigation of an optimised tribocharger design for space resource utilisation

J.N. Rasera [a,b,*], J.J. Cilliers [a], J.-A. Lamamy [b], K. Hadler [a,c]

[a] Department of Earth Sciences and Engineering, Imperial College London, Exhibition Road, London, SW7 2AZ, United Kingdom
[b] ispace Europe S.A, 5, rue de l'Industrie, L-1811, Luxembourg City, Luxembourg
[c] European Space Resources Innovation Centre (ESRIC), Luxembourg Institute of Science and Technology (LIST), Maison de l'Innovation, 5, avenue des Hauts-Fourneuax, L-4362, Esch-sur-Alzette, Luxembourg

ARTICLE INFO

Handling Editor: Dr Olivier Witasse

Keywords:
Tribocharger design
Dry mineral processing
Electrostatic mineral enrichment
Space resource utilisation (SRU)
In situ resource utilisation (ISRU)

ABSTRACT

Triboelectric charging and free-fall separation are attractive technologies for lunar mineral beneficiation. Here, an optimised tribocharger design was built and evaluated under terrestrial conditions. The charging behaviour of pure silica and ilmenite were tested using the optimised design, as were mixtures of silica and ilmenite, and samples of lunar regolith simulant JSC-1. Pure silica and ilmenite acquired negative and positive charge, respectively, through contact with the tribocharger. The tribocharger affected significantly the movement of the pure minerals in the electrostatic field. Results from the binary mixtures indicate that ilmenite recovery is independent of initial ilmenite concentration, and can be predicted from the mass distribution of pure ilmenite samples. For JSC-1, the tribocharger was found to increase the density of the material in certain collectors, indicating an upgrading of denser constituents. The optimised tribocharger design has a significant effect on the charging and separation performance.

1. Introduction

Long-term human missions on the Moon or Mars are aspirations for both space agencies and private corporations. These missions will face long-term sustainability challenges if they are dependent on materials supplied from the Earth. Technologies that will enable the utilisation of locally-available resources are under development. This approach is often referred to as *In Situ* Resource Utilisation (ISRU), or more generally as Space Resource Utilisation (SRU).

Broadly, SRU technologies can be subdivided into the three key stages of the mineral processing flowsheet (Fig. 1). The SRU community has focused historically on excavation and extraction (Rasera et al., 2020). The critical linking stage of beneficiation, however, has received less research attention in comparison (Rasera et al., 2020).

Beneficiation is paramount to the economical operation of mines on Earth. The objective of beneficiation is to produce an optimal, consistent feedstock from the as-mined material for subsequent processing. Beneficiation has significant impact on mining rate, as well as on product yield and energy efficiency (Cilliers et al., 2020). The concentration of the target mineral, referred to as the *grade* (measured in *wt.*%), is increased by raising the quantity of the target mineral and through the removal of waste (*gangue*). The concentration of the target mineral at the process inlet is referred to as the *head grade*. The high-grade output stream is known as the *concentrate*, and the low-grade stream as the *tailings*. The proportion of the original target mineral retained after beneficiation is referred to as the *recovery*. Beneficiation processes aim to achieve a high rejection of waste (increasing grade) whilst minimising losses of desired material to the tailings stream (maximising recovery).

The grade of the as-mined material is often too low to produce metals economically. The target ore can be upgraded to the necessary level for downstream processes through the implementation of beneficiation technologies in the mineral processing flowsheet. These principles will apply equally on the Moon.

All beneficiation technologies separate minerals from waste using differences in physical properties such as density, surface chemistry, or electromagnetic characteristics (Rasera et al., 2020; Wills and Finch, 2015). Gravity-driven beneficiation techniques exploit differences in the mass, density, and/or volume of minerals relative to other ore constituents or process fluids (typically water) to elicit separations. On Earth, mineral processing is largely water-based. For example, technologies such as froth flotation, spiral concentrators, Knelson and Falcon concentrators, and jigs are all dependent on the availability of significant

* Corresponding author. Department of Earth Sciences and Engineering, Imperial College London, Exhibition Road, London, SW7 2AZ, United Kingdom.
E-mail address: j.rasera@imperial.ac.uk (J.N. Rasera).

https://doi.org/10.1016/j.pss.2023.105651
Received 16 December 2022; Received in revised form 6 February 2023; Accepted 7 February 2023
Available online 11 February 2023

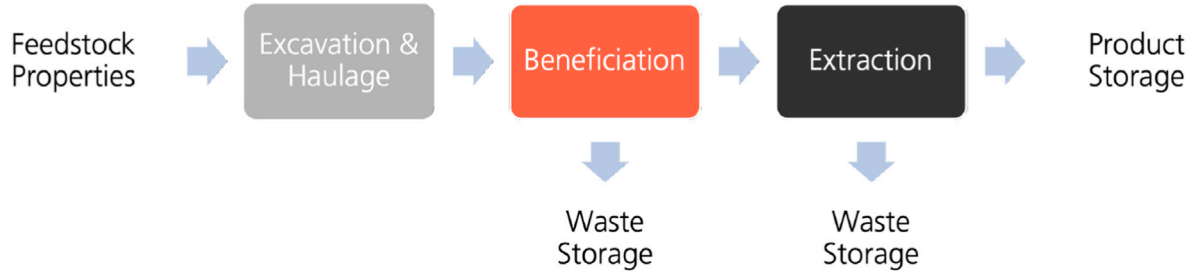

Fig. 1. Mineral processing flowsheet. Adapted from Hadler et al. (Hadler et al., 2020).

quantities of water (Wills and Finch, 2015).

Dry mineral processing technologies have been considered previously (e.g., (Wills and Finch, 2015; Kelly and Spottiswood, 1989a; Kelly and Spottiswood, 1989; Kelly and Spottiswood, 1989b; Manouchehri et al., 2000a; Manouchehri et al., 2000b; Trigwell et al., 2003; Dwari et al., 2009; Bittner et al., 2014; Bilici et al., 2011; Brands et al., 2001; Ballantyne and Holtham, 2010; Ballantyne and Holtham, 2014; Ireland, 2010a; Ireland, 2010b; Ireland and Nicholson, 2011; Ireland, 2012; Lawver and Dyrenforth, 1973; Dwari and Rao, 2007)). The use of dry methods at industrial scale is limited to ilmenite/rutile enrichment from beach sands, iron ore processing, and fly ash cleaning from coal (Wills and Finch, 2015; Bittner et al., 2014; Lawver and Dyrenforth, 1973; Dwari and Rao, 2007).

On the Moon, large-scale, water-intensive methods are not viable: liquid water is not readily available, and costs would be prohibitive to transport any process fluid to the lunar surface. Out of necessity, novel dry processing technologies are required.

Of the dry processing methods explored for SRU in the literature, electrostatic separation techniques have received the greatest attention (Rasera et al., 2020). Electrostatic separators are distinguished by the method of imparting charge on particles. Tribocharging, or triboelectrification, is a method of imparting electrostatic charge on an object by frictional contact. Tribocharging has been observed for thousands of years (Lacks, 2012), however the underlying physical drivers are poorly understood (Lacks and Levandovsky, 2007; Waitukaitis et al., 2014; Zhao et al., 2003). Tribocharging has been demonstrated with success for SRU applications previously (e.g., (Trigwell et al., 2007; Trigwell et al., 2009; Trigwell et al., 2012; Captain et al., 2007; Quinn et al., 2012; Li et al., 1999)).

For separation applications, it is necessary to optimise the design of the tribocharger to maximise the charge transferred to particles of each mineral type. Rasera et al. (2023) demonstrated recently the use of the discrete element method (DEM) for the purposes of tribocharger design optimisation. In their investigation, an optimised design of a tribocharging apparatus was identified based on the relative proportion of particle-wall and particle-particle contacts for single-species PTFE particles with radii of 3.18 mm. The experimental validation presented in their study, however, was limited to relatively large, synthetic polymers, and did not consider granular materials.

The aim of this work is to present an experimental campaign to investigate the suitability of an optimised tribocharger design identified by Rasera et al. (2023) to separating electrostatically dissimilar granular materials. The separation of mixtures of minerals (silica, ilmenite, and lunar soil simulant JSC-1) under laboratory conditions is investigated. Additionally, this work aims to quantify the impacts of both the tribocharger and the inlet feed grade on the separation performance of a free-fall electrostatic separator.

This article is divided into five sections. Following the introduction, Section 2 outlines the theory and development of the electrostatic separator and tribocharger. Section 3 describes the materials and methods. Section 4 presents the results of the investigation and discusses the suitability of the proposed tribocharger design. Finally, Section 5 summarises the main conclusions from this work.

2. Experimental apparatus

2.1. Free-fall separator

In a free-fall separator, charged particles pass through an electrostatic field. Depending on the magnitude and polarity of a particle's charge, they will be attracted towards the electrode of opposing polarity. Because the magnitude and polarity of the charge on any given particle is a material dependent surface property, it is possible to separate different minerals based on how strongly they interact with the electrostatic field.

The theoretical underpinning and final design of the free-fall separator used in this study has been presented by Rasera et al., 2019, 2020. A summary of the underlying theory and its implementation in the design of the free-fall separator is presented here for completeness.

2.1.1. Force balance

The forces acting on particles in a free-fall electrostatic separator are as follows:

$$\sum \vec{F} = \vec{F}_g + \vec{F}_d + \vec{F}_{ad} + \vec{F}_{vdW} + \vec{F}_C + \vec{F}_{dep}, \tag{1}$$

where $\vec{F}_g$ is the gravitational force; $\vec{F}_d$ is the drag force; $\vec{F}_{ad}$ is the adhesion force; $\vec{F}_{vdW}$ is the van der Waals force; $\vec{F}_C$ is the Coulomb force; and, $\vec{F}_{dep}$ is the dielectrophoresis force.

Viscous drag would not be considered for lunar conditions, however it is included here as the experimental campaign described in the subsequent sections was performed under terrestrial atmospheric conditions.

Expanded, Equation (1) becomes:

$$\sum \vec{F}_c = m_i \vec{g} + 0.5\rho_f \vec{v}_i^2 C_d A + \frac{q_i}{4\pi\epsilon_0}\sum_{j=1}^{n}\frac{q_j(\vec{R}_i - \vec{R}_j)}{|\vec{R}_i - \vec{R}_j|^3} + \frac{A_H S^2 (r_i r_j)}{48\Omega^2 (r_i + r_j)} + q_i \vec{E} + 2\pi r_i^3 \epsilon_0 \left(\frac{\epsilon_i - \epsilon_0}{\epsilon_i + 2\epsilon_0}\right)\nabla \vec{E}^2. \tag{2}$$

where m_i is the mass of the particle in kg; $\vec{g}$ is the acceleration due to gravity in m/s^2; ρ_f is the density of the fluid (here, air) in kg/m^3; $\vec{v}_i$ is the particle velocity in m/s; C_d is the drag coefficient; A is the cross sectional area in m^2; r_i and r_j are the radii of particles i and j in m; q_i and q_j are the charges on particles i and j in j in C; ϵ_0 is the vacuum permittivity in F/m; $\vec{R}_i$ and $\vec{R}_j$ are the relative position vectors of particles i and j in m; A_H is the Hamaker constant ($4.3 \times 10^{-20} J$); S is the surface cleanliness; Ω is the diameter of an oxygen atom ($1.32 \times 10^{-10} m$), considered to be the minimum separation of two particles on the Moon (Perko et al., 2001); and, $\vec{E}$ is the electrostatic field vector in V/m.

It should be noted that the third term in Equation (2) assumes that the charge is located at a particle's centroid. Whilst this is not physically realistic, it is considered a reasonable assumption for modelling purposes (Laurentie et al., 2010, 2013; Kolehmainen et al., 2017a, 2017b; Sippola et al., 2018). Furthermore, a planar electrostatic field geometry is assumed in this work, however other geometries are possible.

2.1.2. Separator design

The charge acquired by any given particle is material-dependent (Cruise et al., 2022), and this property is leveraged by electrostatic beneficiation methods to elicit separations by type. The operating principle of an electrostatic separator, therefore, is to make the Coulomb force from Equations (1) and (2) dominant, in order to affect significantly the horizontal component a particle's motion.

The free-fall separator (Fig. 2) used in this study was based on the designs employed by Trigwell et al., 2009, 2012, Captain et al. (2007), and Quinn et al. (2012) for investigating free-fall separation of lunar regolith simulants. The apparatus employed here used a programmable FLS40 linear stage from Fuyu Technology to precisely control the position of the two 320 by 150 mm (height and width, respectively) copper electrodes. Each electrode is powered by an XP Glassman FJ60-series high-voltage DC power supply. These features allow for detailed investigations into the effect of field strength, electrode voltage, and electric field geometry.

For the purposes of this study, a quasi-planar electrostatic field is preferable to a non-uniform field. This was chosen to minimise the number of variables that could potentially impact the separation performance beyond the contributions of the tribocharger itself.

A removable aluminium collector is mounted on a fixed frame at the bottom of the separator box (Fig. 3). The collector has seventeen 2-cm-wide by 3.5-cm-deep channels, eight positive collectors, (left to right: P8 to P1), a central collector (0), and negative collectors (N1–N8). This design allows for high-fidelity analysis of the samples collected.

The separator is contained within a Faraday cage for electrical safety, and to minimise inductive interference from external sources. Particles are fed into the separator using a grounded Eriez FT0B linear vibratory feeder. As the particles leave the feeder, they pass in front of a Simco-Ion MEB bar to neutralise as much residual charge as possible. The particles are then guided into the separator via the tribocharger by a grounded aluminium funnel (see Fig. 4).

2.2. Tribocharger design

A tribocharger design employed previously with success in the literature is described by Trigwell et al., 2009, 2012 and Quinn et al. (2012). In these works, the authors looked to enrich the mineral ilmenite from lunar regolith simulants using a static tribocharger and free-fall electrostatic separator. Their design consisted of an aluminium tube with a series of twisted aluminium baffles suspended inside, as shown in Fig. 5. The design details of the baffles employed in these studies, however, are

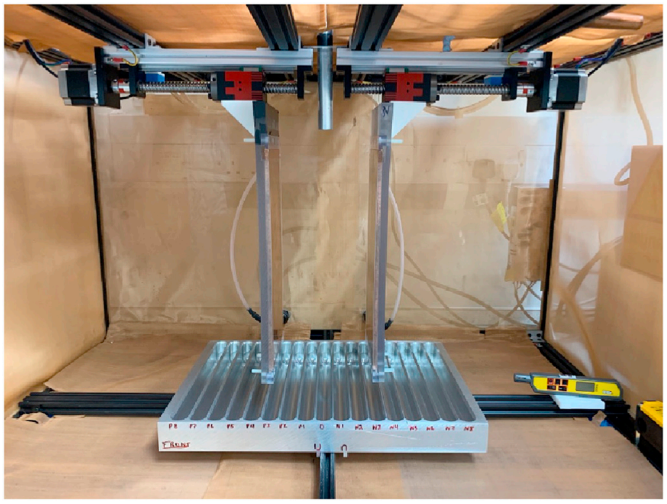

Fig. 2. The free fall triboelectric separator built for this investigation, adapted from the designs of Trigwell et al. (Trigwell et al., 2009, 2012), Captain et al. (Captain et al., 2007) and Quinn et al. (Quinn et al., 2012).

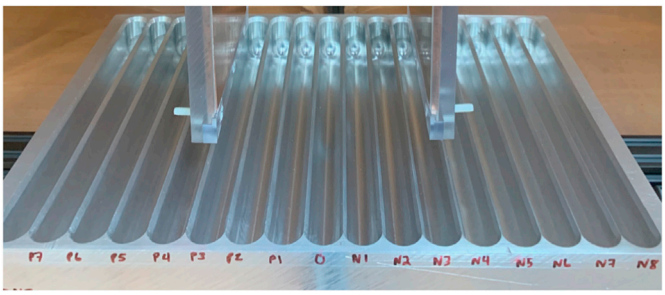

Fig. 3. The machined aluminium collector mounted in situ within the separator. Positively charged particles report to the N bins, and negatively charged particles report to the P bins. Collectors are labelled from left to right: P8 to P1 – 0 – N1 to N8.

Fig. 4. The feeder arrangement employed in this study. The FT0B linear vibratory feeder conveys particles to the injection point. Here, the Simco-Ion MEB bar emits ions to neutralise any preexisting charge. The falling particles are then guided into the separator by the aluminium funnel.

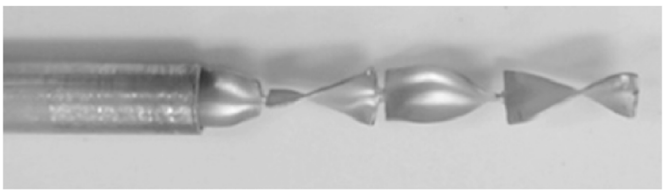

Fig. 5. The tribocharger design employed by Trigwell et al. (Trigwell et al., 2009, 2012) and Quinn et al. (Quinn et al., 2012).

not specified; the pitch angle appears to be ~90°, however the length of each segment is unknown.

Rasera et al. (2023) identified two primary design criteria to optimise the design of a tribocharger in order to maximise the charge acquired per unit mass of the particles:

1. Particle-wall contacts should be maximised; and,
2. Flow density should be kept to a minimum.

Through their application of the discrete element method, Rasera et al. (2023) identified a twisted baffle tribocharger with a pitch of 6 cm (a pitch angle of 270°, compared to the ~90°design employed by Trigwell et al. and Quinn et al.) as an optimal design. This design was found to maximise the particle-wall contact area whilst ensuring good material throughput at low inlet mass flow rates.

The design proposed by Rasera et al. (2023) was optimised for ideal, relatively large, PTFE spheres, not granular materials. As a result, the design is not necessarily the optimal one for charging silica, ilmenite, and JSC-1, particularly for the 150–250 μm size fractions used here. The aim of the present study is to evaluate the impact of the optimised design on the separation performance of these granular materials, not to validate the optimisation of the tribocharger design.

In this work, the same basic design used by Rasera et al. (2023) is employed. The baffle has a diameter of 1.9 cm, however a longer charger baffle and guide tube are employed (11.25 cm and 13.5 cm, respectively) to provide greater internal surface area for contact charging. The tube was made from 6063T6-grade aluminium, and the baffle from 1050A-grade aluminium. Tailored surface finishes were not used. The dimensions were limited by internal geometry of the separator, and to minimise the interaction of the charger with the electrostatic field.

The charger design used in this work cannot bring the particles to their saturation limit. However, attaining saturation charge is not necessary to perform separations successfully. Following Equations (1) and (2), the Coulomb force is dependent on both the charge on the particle as well as the strength of the electrostatic field. Highly charged (i.e., saturated) particles can be separated by a relatively weak electrostatic field. Conversely, weakly-charged particles can be separated by a strong field.

3. Materials and methods

This section summarises the preparation of the test samples, as well as the experimental protocols used.

3.1. Sample preparation

Crushed, 99.8%-pure silica (quartz) sand from Fisher Scientific, and pure ilmenite acquired from a mine in Guinea, were used in this study. Both materials were dry sieved to isolate the 150–250 μm fraction using a Retsch Sieve Shaker AS 200 Control. This size fraction was employed as it was the smallest fraction shared by all of the materials used in this study. The sieved samples were then analysed using a Malvern Panalytical Mastersizer 3000E with the Hydro EV accessory. The size distribution curves are found in Fig. 6. The silica was found to have a D_{50} of 242 μm; the ilmenite was found to have a D_{50} of 226 μm. Three 15-*g* samples of JSC-1 (McKay et al., 1994) lunar regolith simulant were studied. The simulant was sieved to isolate the 150–250 μm fraction; the size distribution for the sample can be found also in Fig. 6. The JSC-1 retained a higher fraction of fine (<100 μm) particles compared to the silica and ilmenite samples. The D_{50} was found to be 205 μm.

Binary mixtures comprising 5%, 10%, 15% and 20% ilmenite by mass were also used. Prepared samples were stored in a desiccator with silica gel desiccant to prevent the adsorption of water onto the particles. Each samples had a total mass of 20 *g*. Each test was repeated three times with a new samples.

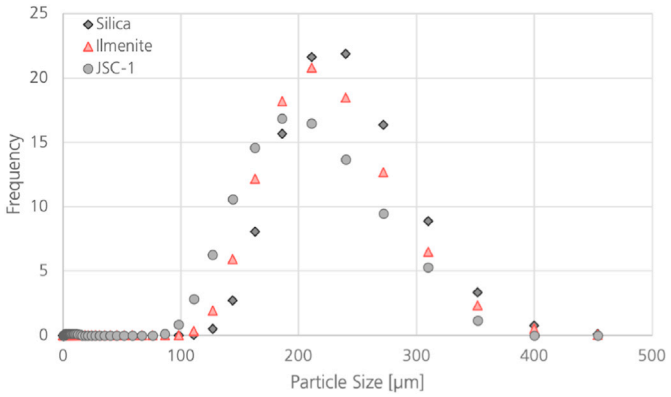

Fig. 6. Particle size distributions of sieved silica, ilmenite and JSC-1.

3.2. Separator parameters

The electrodes were separated by a distance of 150 mm, and the electrode voltage was set to ± 25 kV. This arrangement resulted in a quasi-planar field geometry. These set points resulted in a field strength of approximately 333 kV/m. For comparison, this field strength is approximately 45% greater than the field used by Trigwell et al. (2012) (±15 kV separated by 160 mm, or 187.5 kV/m), and around 25% greater than the maximum field used by Quinn et al. (2012) (±20 kV separated by 160 mm, or 250 kV/m).

The FT0B vibratory feeder was set up to produce an average feed rate of 0.2 g/s; this was the lowest feed rate achievable across all samples with the equipment employed in this study. The relative humidity within the lab during testing ranged from 28% to 35%, and the ambient temperature was between 20 and 22 °C. Temperature and humidity were monitored using a Kane DTH10 thermohygrometer. The ambient humidity within the lab was not controlled, however it was kept to a minimum through the use of a portable dehumidifier. Testing was conducted over the course of a week.

Prior to each test, the system was aligned. The alignment was performed by passing the material using the vibratory feeder through both the baffled and unbaffled tubes without the electrostatic field. In both cases, the majority of particles reported to the central collector channel, however some material reported to the P1 and N1 collectors. The system was considered aligned once the mass reporting to the P1 and N1 collectors was equal. For the baffled case, the end of twist was installed perpendicular to the length of the collector channels to minimise the effects of initial particle velocity on the separation performance.

3.3. Mineral separation procedure

Each test was performed using the same procedure as follows:

1. Shut the separator access panel and confirm safety interlocks are engaged.
2. Energise the electrodes.
3. Place the test sample onto the conveyor for the vibratory feeder.
4. Engage the feeder and Simco-Ion MEB bar.
5. Power-down the equipment when the feeder was empty.

Once the safety interlocks had released the access panel, the collection hopper was removed, and the samples from each channel were collected individually in aluminium sample dishes for subsequent grade and recovery analysis.

3.4. Charge measurement

Bulk charge is measured easily and is indicative of the charging behaviour of the entire sample. However, bulk charge measurements do

not provide any insight to the charging behaviour of individual particles (Rasera et al., 2022, 2023). Only the bulk charge of the pure mineral samples was measured in this study since it is not representative of charger performance. This was done to enable comparisons of the charging behaviour with previous works.

The bulk charge of each pure mineral sample was measured by feeding particles through the tribocharger into a Faraday cup connected to a Keithley 6517b electrometer. All measurements were repeated at least three times.

As only one electrometer was employed in this study, the initial charge was measured by passing the sample through the apparatus without the tribocharging baffle. The overall change in charge, dq, was found by taking the difference between the baffled and unbaffled measurements.

3.5. Grade and recovery analysis

The grade, η, of ilmenite in the binary mixture tests can be evaluated from the bulk density. The bulk density of the material reporting to each collector was evaluated using a Micrometrics AccuPyc II 1340 Helium Pycnometer. The densities of the pure silica, ρ_{silica}, and ilmenite, $\rho_{ilmenite}$, were measured to be 2.65 g/cm^3 and 4.57 g/cm^3, respectively. These densities were then used to evaluate the grade of ilmenite present in each sample as follows:

$$\eta = \frac{\rho_{ilmenite} \times \left(\frac{\rho_{silica}}{\rho_{sample}} - 1\right)}{\rho_{silica} - \rho_{ilmenite}} \tag{3}$$

Since the initial concentrations for each sample, $m_{ilmenite,in}$, are known, the recovery is determined as follows:

$$recovery = \frac{m_{collector} \times \eta}{m_{ilmenite,in}}, \tag{4}$$

where $m_{collector}$ is the total mass of material in any given collection channel.

For the JSC-1 samples, it was not possible to evaluate the mineralogy of the collected material by bulk density alone as it is not a binary mixture. Instead, the bulk density was measured in order to infer what, if any, mineral upgrading occurred. If the density is found to increase, this would indicate an increase in the concentration of the denser constituents, and *vice versa*.

4. Results and discussion

This section presents and discusses the results of the experimental campaign. All data were analysed statistically two-tailed Student's *t*-Test assuming $\alpha = 0.05$. Insufficient material was collected in collectors P8–P4 and N2–N8 for individual analysis. Any material reporting to collectors beyond P3 were incorporated into that sample. Any material reporting to collectors beyond N1 was incorporated similarly.

4.1. Pure minerals

Initial tests were performed on pure mineral samples. It is imperative that the tribocharger maximise particle-wall contacts in order to elicit horizontal motion within the electrostatic field, as there are effectively no differences in the material properties of the particles in pure samples.

The mass distributions are presented in Fig. 7, and an example of the separator results are found in Fig. 8. The presence of the tribocharger baffle has a statistically significant impact on the distribution of material for both silica and ilmenite. An appreciable change in the distribution of material is apparent.

It is observed that silica particles tend to gain primarily negative charge through contact with aluminium. In contrast, the ilmenite is found to spread both towards the positive and negative electrodes. The more

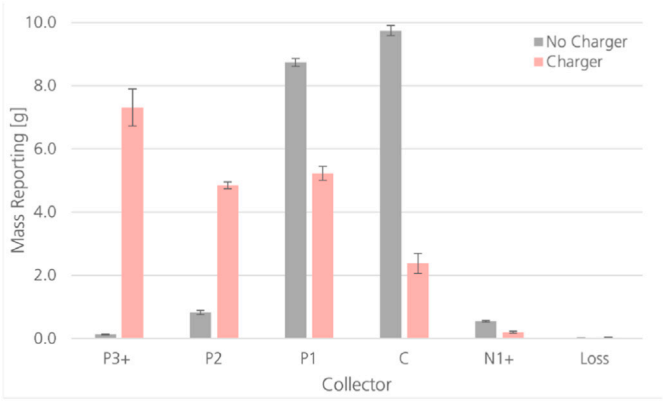

(a) Silica mass distribution by collector.

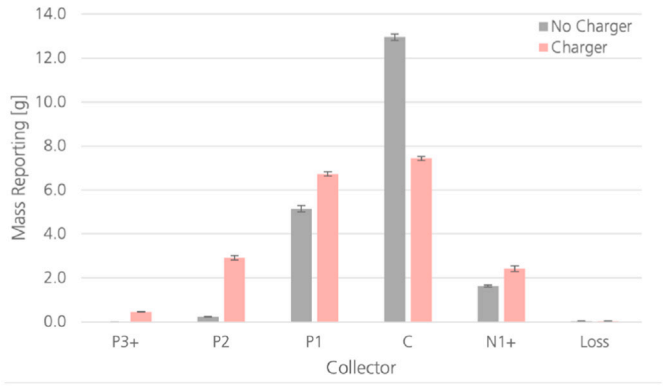

(b) Ilmenite mass distribution by collector.

Fig. 7. Comparison of the no charger and charger mass distributions for pure silica and ilmenite samples. Error bars indicate 95% confidence intervals. All measurements found to be statistically significant.

limited spread of the ilmenite is explained partially by the its greater density (and greater inertia) compared to silica (4.57 g/cm^3 vs 2.65 g/cm^3). The distribution of particles towards both the positive and negative electrodes could be explained by high particle-particle contacts. However, as a similar effect is not seen with the silica samples, and since the inlet feed rates were the same, it is unlikely that a substantial increase in particle-particle contacts occurred. Furthermore, the presence of the tribocharger would reduce the vertical component of the particle motion, which may have been sufficient to enable a greater degree of horizontal motion before reaching the collectors. This effect may be partially responsible for the distribution of silica as well. Future studies should aim to control the vertical component of particle velocity.

The bulk charge of both the silica and ilmenite samples are presented in Fig. 9. In this plot, the silica samples gain clearly negative charge, whereas the bulk charge of the ilmenite samples barely changes at all. These findings are in agreement with those presented previously in literature. Ferguson (2010) produced a triboelectric series of heavy minerals by analysing inductive separation data. Here, silica was found to be highly electronegative, and thus a strong collector of negative charge. In contrast, ilmenite was found to be weakly electropositive, gaining a small amount of positive charge. Gooding and Kaufman (2011) produced a comprehensive triboelectric series showing similar behaviours of ilmenite and silica.

In another study, Yang et al. (2018) measured the impact of different charger materials on the tribocharging process, and found that ilmenite tended to charge slightly positively on conductors (copper and steel). These results are explained by the relative similarity of the work functions of ilmenite (4.29 ± 0.11 eV (Li et al., 2016)), copper (4.42 eV (Wilson, 1966) to 4.65 eV (Trigwell et al., 2007)), aluminium (4.28 eV

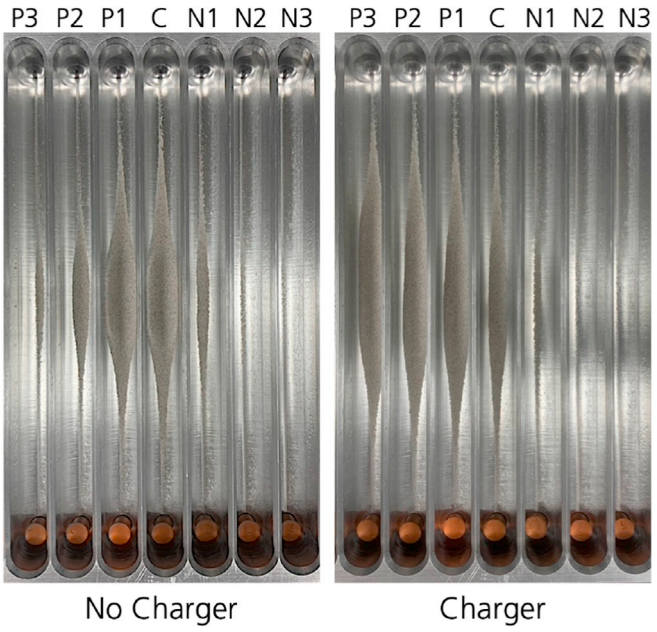

(a) Silica.

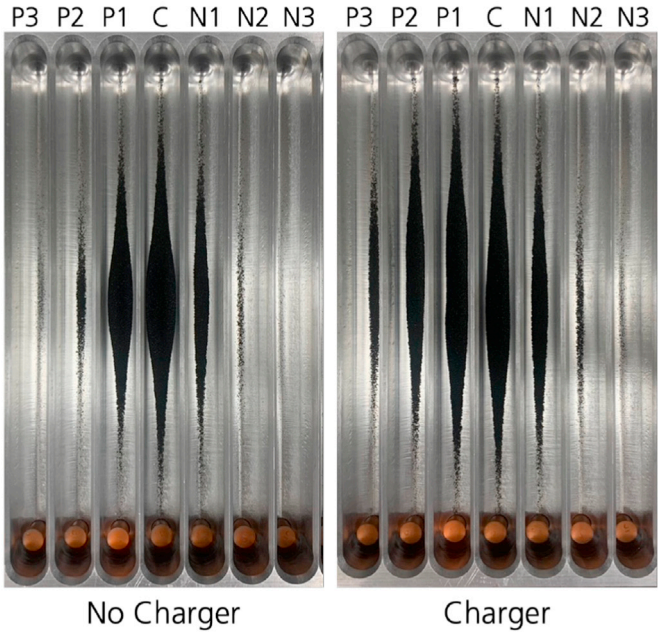

(b) Ilmenite.

Fig. 8. Visual comparison of the impact of the charger on pure silica (a) and ilmenite (b).

(Trigwell et al., 2007)), and stainless steel (4.34 eV (Wilson, 1966) to 5.01 (Trigwell et al., 2007)). Following Schein et al. (1992), Matsusaka et al. (2000), Laurentie et al., 2010, 2013, and Kolehmainen et al., 2016, 2017a, 2017b charge transfer between conductors (or semiconductors) is described by:

$$\Delta q = \Delta A \kappa_c \epsilon_0 \left(\frac{\varphi_i - \varphi_j}{\delta_e e} - \vec{E}_{contact} \cdot \hat{n}_{ij} \right), \tag{5}$$

where ΔA is the change in contact area for a given interaction; κ_c is the empirically-derived charging efficiency; ϵ_0 is the permittivity of free space; δ_e is the separation distance between two particles at which point charge transfer ceases; e is the magnitude of the electron charge; φ_i and φ_j are the effective work functions for conductors and semi-conductors (including ilmenite); $\vec{E}_{contact}$ is the electrostatic field at the point of contact; and, $\hat{n}_{ij}$ is the unit normal vector pointing from particle i to j at the point of contact. In cases where the differences in work functions are small or negligible, the net charge transfer measured in the bulk sample would be minimal, as observed.

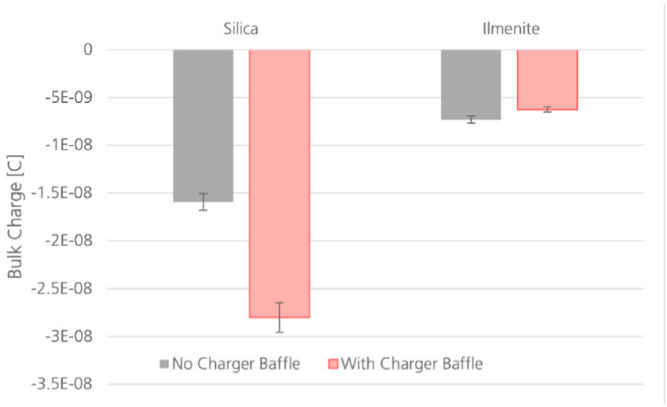

Fig. 9. Differences in bulk charge between the no charger and with charger arrangements.

Finally, it is important to note that, despite the relatively minuscule change in bulk charge for ilmenite, the change mass distribution is appreciable and statistically significant. This adds further support to Rasera et al.'s (Rasera et al., 2022, 2023) argument that bulk charge is, at best, indicative only, and fails to capture the underlying distribution of individual particle charges.

4.2. Binary mixtures

The grade-recovery relationships for the experiments conducted with and without the tribocharger baffle are found in Fig. 10. For all of the samples in the case without the charger baffle, the majority of material reported to the centre collector (Fig. 11). This results in consistently high ilmenite recovery in this channel, albeit at a relatively low grade. There is some upgrading of ilmenite in the negative collector channels (N1+), however the recovery is consistently low (~9%).

When the tribocharger baffle is introduced, significant changes in the grade-recovery curve occur. High grades (65%–89%) of ilmenite reported to the N1+ collectors with nearly double the recovery of the case without the tribocharger baffle. These results suggest that a single pass using the tribocharger arrangement would be sufficient to produce significant upgrading of ilmenite in a bulk processing situation, assuming low recovery is acceptable. This would likely be the case for early SRU demonstrations on the Moon. For an early SRU demonstration, the main priority would likely be attaining the necessary grade for the downstream reduction step rather than minimising waste.

Nearly pure silica (average of ~ 1.3 *wt%* ilmenite) was found to report to the P3+ collector in all tribocharger cases. Further, the net mass recovery of material in this channel is approximately 33% of the total sample mass. For mineral processing flowsheets where recovery is a driving factor (i.e., terrestrial mines), these results suggest that the inclusion of a reprocessing circuit could produce very high grade material through gangue rejection whilst minimising ore loss.

The results for both cases indicate consistently that the recovery of ilmenite across all collectors is largely independent of the head grade. However, this is not the case for the concentrate grade: higher head grade consistently results in higher concentrate grades.

Fig. 12 compares the recovery of both silica and ilmenite for each mixture to the mass recovery of the pure mineral samples. There is

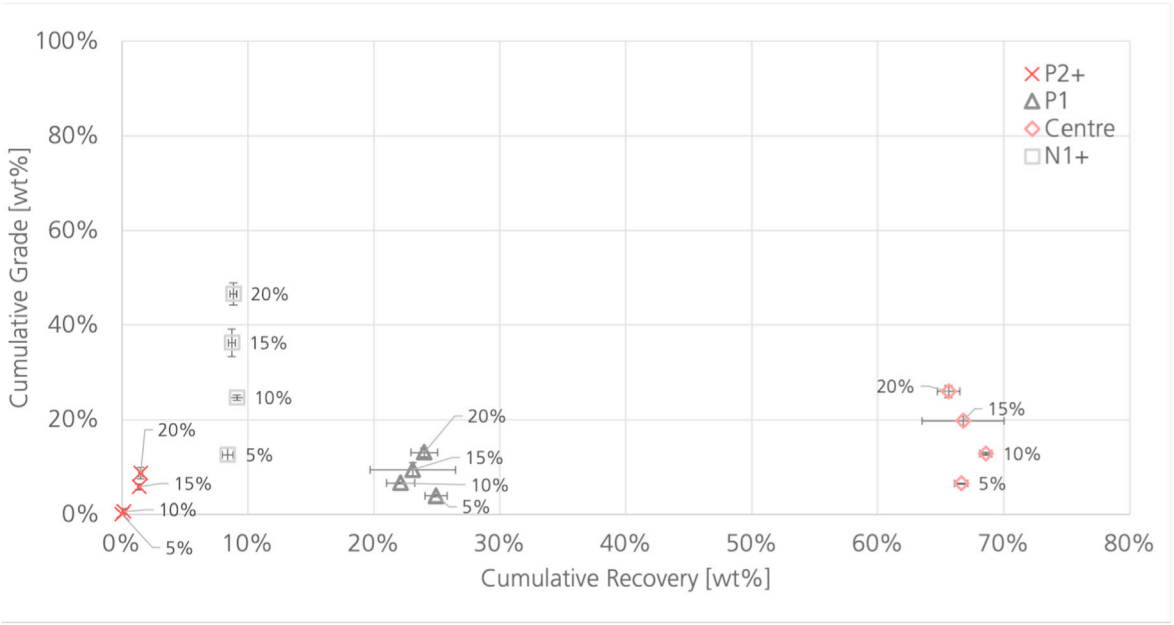

(a) No charger arrangement.

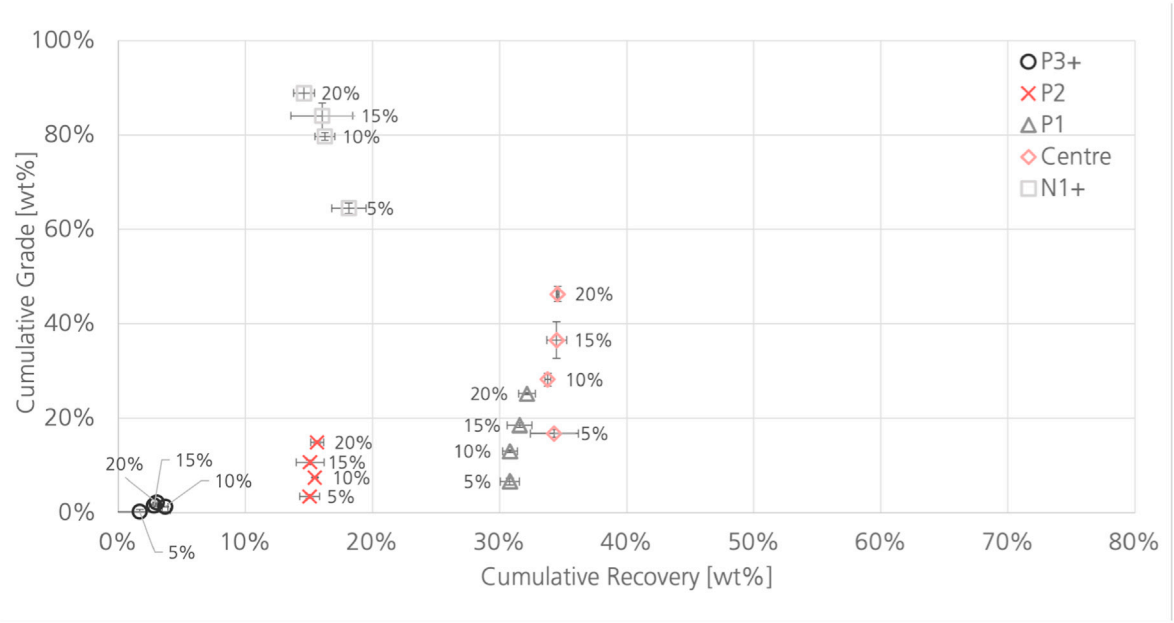

(b) With charger arrangement.

Fig. 10. Comparison of the unbaffled and baffled grade-recovery curves for the binary mixtures of silica and ilmenite, arranged by collector channel. For each data set, the head grade decreases from top (20 *wt%*) to bottom (5 *wt%*). All error bars indicate 95% confidence intervals.

excellent agreement between the overall recovery trends. There are also relatively small absolute differences between the mass recoveries of the pure minerals and the recoveries from the mixtures. This suggests that the optimised tribocharger design is maximising successfully the desirable particle-wall interactions described by Rasera et al. (2022, 2023). Had the recoveries not demonstrated such an agreement, it would indicate that particle-particle contacts were contributing significantly to the overall charging behaviour of the sample.

4.2.1. *Reprocessing study*

The data collected for each mixture can be used for an illustrative tailings reprocessing study. This study is highly idealised, however it demonstrates the possible impact of the reprocessing of the tailings stream on the overall recovery of ilmenite. The grade and recovery characteristics measured experimentally are assumed to be approximately linear, based on the data reported in Fig. 10b. Each reprocessing step would see the total mass of the tailings fed into the system at a constant flow rate of 0.2 g/s, per the experimental campaign.

With a starting grade of 20% ilmenite, the grade of the concentrate following electrostatic separation is around 89%, recovering only 16% of the total ilmenite available. The tailings stream, therefore, would have an ilmenite grade of 17%, with 84% of the initial ilmenite. Interpolating linearly from the experimental data, the grade and recovery for each reprocessing step is calculated until the tailings grade falls below 5%, the limit of the experimental data. The results of this analysis are presented in Fig. 13.

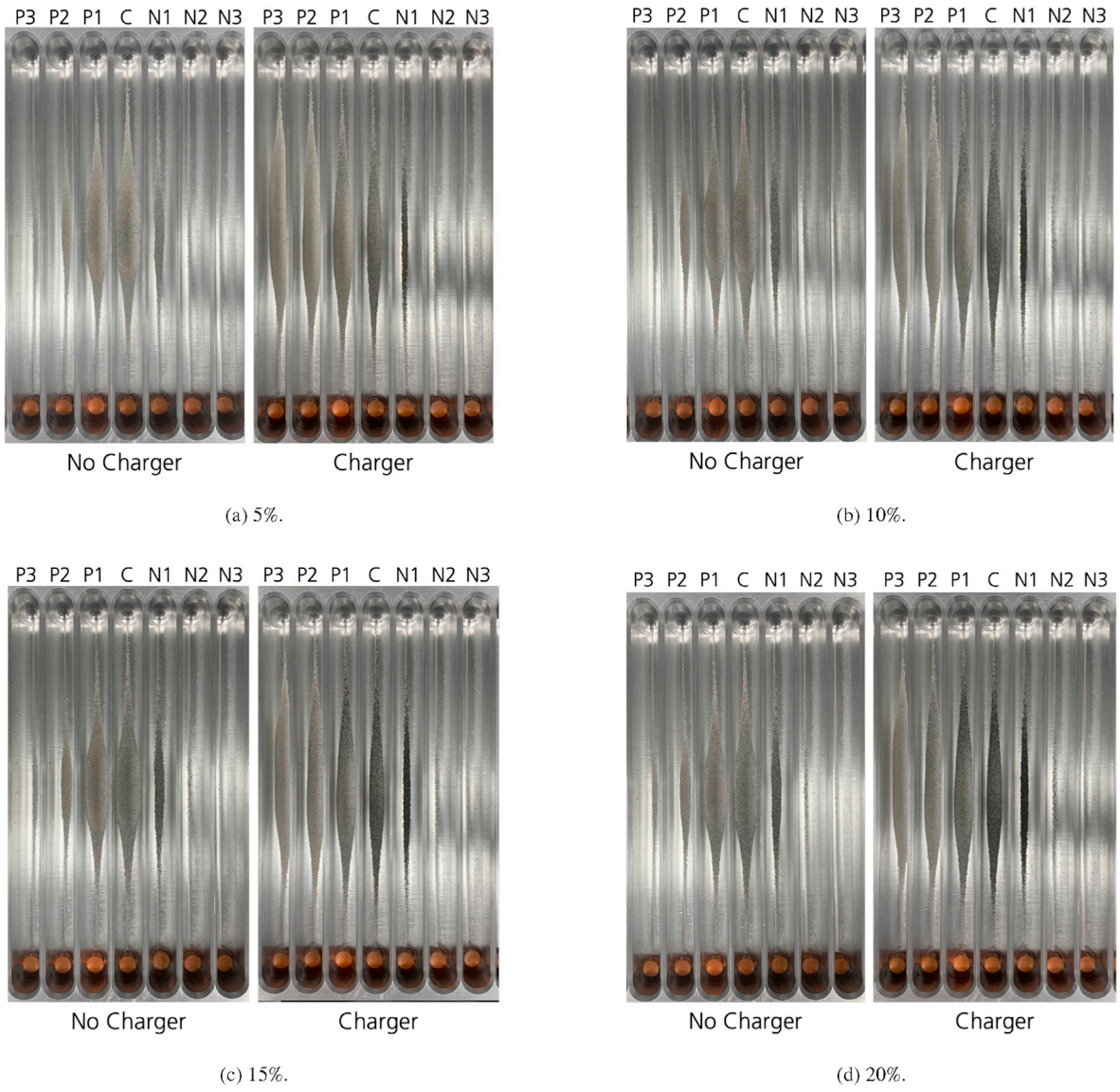

Fig. 11. Visual comparison of the impact of the charger on the mixtures of different initial concentrations.

These results indicate that following 10 rounds of reprocessing, the concentrate grade of ilmenite would be around 75%, with a net ilmenite recovery of 83%. In practice, the number of reprocessing steps would be determined by factors such as the required grade for the subsequent processing step, or the necessary level of ore recovery.

For complex mixtures, such as the lunar regolith or many naturally-derived regolith simulants, grade and recovery would not be linear, as factors such as particle size and mineral liberation would affect the relationship. However, for this binary mixture, it is a reasonable way of demonstrating the concept of staged processing. This is only one example of a reprocessing scheme. The experimental data indicated that the P3+ collectors contained approximately 37% of the total silica in any given sample, with a silica grade exceeding 98%. Another reprocessing scheme could remove this high-grade silica, and enrich subsequently the ilmenite-bearing streams.

4.3. JSC-1

The tribocharger employed in this study is optimised for an idealised feedstock, and therefore it is not expected to have a significant effect on simulant, which is a complex mix of sizes, shapes and mineral types.

The bulk densities of the unbeneficiated JSC-1 sample and for each collector channel are reported in Fig. 14. In this case, the material was tested with the tribocharger baffle only; the impact of the charger on the binary mixtuers had already been established, and detailed mineralogical analysis of the material was not possible. To evaluate the effect that tribocharger was having on the JSC-1 samples, bulk densities are analysed to gain insight into the underlying behaviour of the sample.

The density of the unbeneficiated bulk sample was measured to be 2.95 g/cm^3. JSC-1 is comprised predominantly (69%, modal area) of lower-density plagioclase (35% (Schrader et al., 2010); $2.2 < \rho < 2.6$ g/cm^3 (King) and glass (34% (Schrader et al., 2010); $2.1 < \rho < 2.8$ g/cm^3 (Yamada and Shoji, 1990)), with the balance made up of higher-density constituents, namely pyroxene (12% (Schrader et al., 2010); $3.0 < \rho < 4.0$ g/cm^3 (Kinga)) and olivine (14% (Schrader et al., 2010); $3.2 < \rho < 4.4$ g/cm^3 (Kingb)). If the bulk density of a collector channel is statistically lower or higher than the unbeneficiated sample, it implies that upgrading of some form has occurred.

There were no statistically significant differences between the bulk densities of the P3+ to centre collectors, nor between those channels and the bulk sample density (Fig. 14). However, there was a statistically significant increase to the bulk density of the material reporting to the N1+ collector. An average of 5% of the total sample mass reported to these collectors. Similar material movements for JSC-1 charged on

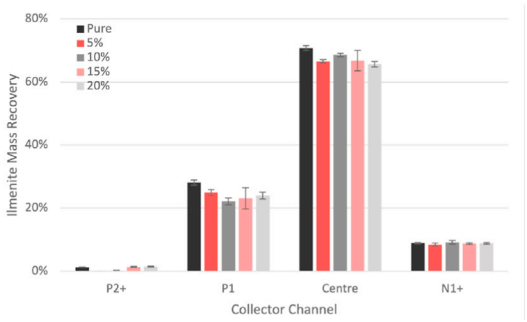

(a) Ilmenite mass recovery, no charger.

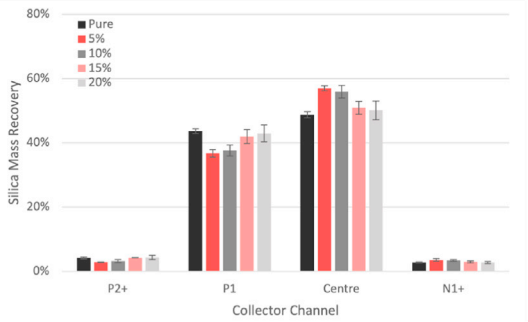

(b) Silica mass recovery, no charger.

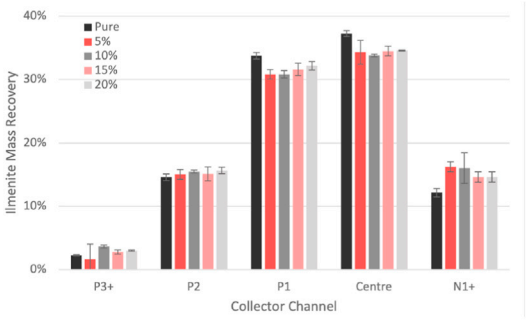

(c) Ilmenite mass recovery, with charger.

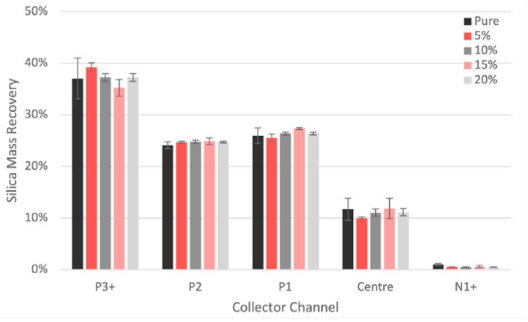

(d) Silica mass recovery, with charger.

Fig. 12. Comparison of the ilmenite and silica mass recovery by collector channel for both binary mixtures and pure samples. There are statistically significant differences between the mass recovery of the pure minerals versus the different samples in most cases. However, the absolute differences between the mass recoveries are relatively minor. The mass recoveries of the mixtures agree strongly with the trends set by the pure samples for both materials.

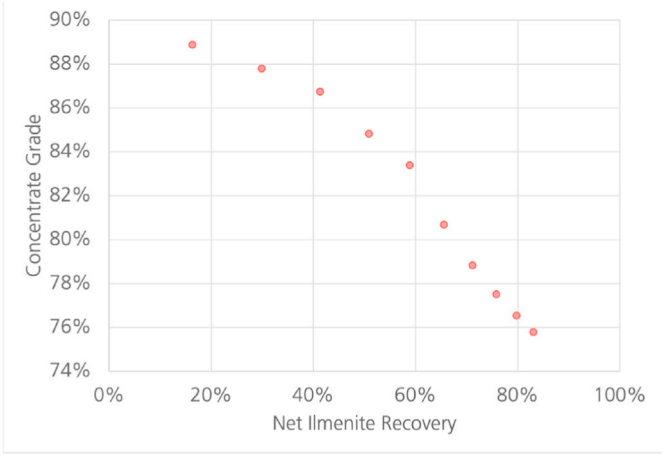

Fig. 13. An example tailings reprocessing to increase the overall recovery of ilmenite. As the recovery is increased through reprocessing, the concentrate grade decreases.

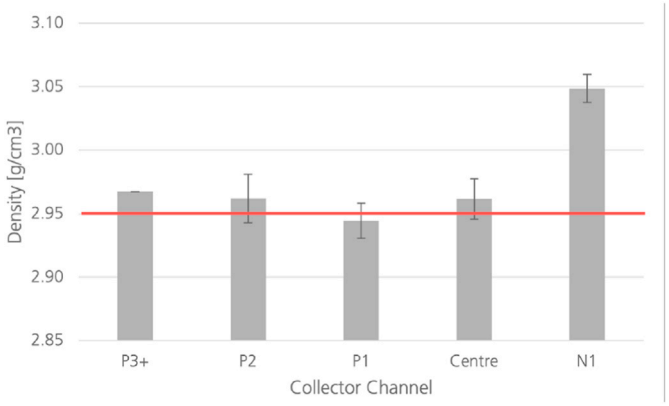

Fig. 14. Density measurements for the JSC-1 samples by channel. There was insufficient material to accurately measure the P3+ density, so the three samples were combined and measured together. The horizontal line indicates the density of the bulk sample. All error bars indicate 95% confidence intervals. A statistically significant increase in the density was observed for the N1+ channel.

aluminium were reported by Trigwell et al. (2007), albeit with a different charger arrangement. This suggests that the optimised charger design is concentrating successfully some combination of the higher-density constituents of JCS-1 in the N1+ channels, despite being optimised for an idealised feedstock. Further mineralogical characterisation is required to confirm this.

5. Conclusions

In this work, the optimised tribocharger design identified by Rasera et al. (2023) was built and tested under laboratory conditions using granular materials.

Experimental results using the pure silica demonstrating a clear tendency to acquire negative charge through contact with aluminium. The pure ilmenite samples were found to gain both positive and negative charge, enabling appreciable material movement in the electrostatic field, whilst experiencing negligible change in bulk charge. Both of these findings are in agreement with the material charging behaviours presented previously in the literature.

When the binary mixtures were charged using the optimised design, statistically significant increases in the grade and recovery of the ilmenite were found compared to the cases where the charger was not used. The mass recovery of ilmenite was found to be largely independent of the

sample initial concentration, while the concentrate grade was dependent on it. The charger was found to decrease significantly the grade of ilmenite in the P3+ collector to negligible levels whilst collecting around 1/3 of the total sample material. This indicates that reprocessing of the material could result in significant upgrading through gangue rejection. Further, an indicative reprocessing study shows that recovery can be increased appreciably through the bulk reprocessing of the tailings channels.

A notable finding from this study is that the mass recovery of both silica and ilmenite from the binary mixtures was found to track closely the mass recovery trends of the pure ilmenite and silica samples. This suggests that the optimal design is maximising desirable particle-wall contacts.

The tribocharger had been optimised for an idealised feedstock, and so was not expected to have a significant impact on the JSC-1 sample. The results for these tests were less clear than for the binary mixtures, however the N1+ channels recorded a modest, but statistically significant, increase in density compared to the other collectors as well as to the unbeneficiated sample. These data agree generally with previous findings in the literature, however further modal and/or geochemical analysis is required to confirm this.

The findings presented here indicate that the optimised design identified previously by Rasera et al. (2023) is capable of producing statistically significant increases in the grade of the target minerals.

This study was conducted under terrestrial laboratory conditions, using a tribocharger optimised for synthetic, idealised materials. Future studies should consider the optimisation of a tribocharger using data from real minerals. Furthermore, it would be advantageous to study the efficacy of such a charger under simulated lunar conditions (high vacuum, lower gravity, higher/lower temperatures, etc.), where possible.

CRediT authorship contribution statement

J.N. Rasera: Conceptualisation, Experimental Methodology and Investigation, Data Analysis, Manuscript Writing, Editing and Revision. J.J. Cilliers: Supervision, Funding and Resource Acquisition, Manuscript Editing and Revision. J.-A. Lamamy: Supervision, Industrial Partner. K. Hadler: Supervision, Manuscript Editing and Revision.

Declaration of competing interest

The authors declare that they have no known competing financial interests or personal relationships that could have appeared to influence the work reported in this paper.

Data availability

Data will be made available on request.

Acknowledgements

This research has been made possible through the support of the Luxembourg National Research Fund (FNR) under Industrial Fellowship Grant 12489764.

The authors acknowledge the support of the Natural Sciences and Engineering Research Council of Canada (NSERC) [ref: 411291661]. Cette recherche a été financée par le Conseil de recherches en sciences naturelles et en génie du Canada (CRSNG), [réf: 411291661].

The authors would like to thank Mr S.O. Starr for his valuable feedback and insights.

References

Ballantyne, G.R., Holtham, P.N., 2010. Application of dielectrophoresis for the separation of minerals. Miner. Eng. 23, 350–358. https://doi.org/10.1016/j.mineng.2009.09.001.

Ballantyne, G.R., Holtham, P.N., 2014. Evaluation of the potential for using dielectrophoresis to separate minerals. Miner. Eng. 55, 75–79.

Bilici, M., Dascalescu, L., Dragan, C., Fati, O., Iuga, A., Samuila, A., 2011. Tribocharging and electrostatic separation of mixed granular solids in fluidized bed devices. IEEE Trans. Dielectr. Electr. Insul. 18, 1476–1483.

Bittner, J.D., Hrach, F., Gasiorowski, S., Canellopoulus, L., Guicherd, H., 2014. Triboelectric belt separator for beneficiation of fine minerals. Procedia Eng. 83, 122–129.

Brands, L., Beier, P., Stahl, I., 2001. Electrostatic Separation. Wiley Online Library, pp. 423–441.

Captain, J., Trigwell, S., Arens, E., Biris, A., Captain, J., Quinn, J., Calle, C., 2007. Tribocharging lunar simulant in vacuum for electrostatic beneficiation. AIP. In: AIP Conference Proceedings, vol. 880, pp. 951–956.

Cilliers, J.J., Rasera, J.N., Hadler, K., 2020. Estimating the scale of space resource utilisation (SRU) operations to satisfy lunar oxygen demand. Planet. Space Sci. 180, 104749.

Cruise, R.D., Hadler, K., Starr, S.O., Cilliers, J.J., 2022. The effect of particle size and relative humidity on triboelectric charge saturation. J. Phys. Appl. Phys. https://doi.org/10.1088/1361-6463/ac5081.

Dwari, R., Rao, K.H., 2007. Dry beneficiation of coal—a review. Miner. Process. Extr. Metall. Rev. 28, 177–234.

Dwari, R., Rao, K.H., Somasundaran, P., 2009. Characterisation of particle tribo-charging and electron transfer with reference to electrostatic dry coal cleaning. Int. J. Miner. Process. 91, 100–110.

Ferguson, D., 2010. A basic triboelectric series for heavy minerals from inductive electrostatic separation behaviour. J. S. Afr. Inst. Min. Metall 110, 75–78.

Gooding, D.M., Kaufman, G.K., 2011. Tribocharging and the triboelectric series. Encycl. Inorg. Bioinorg. Chem. 1–9.

Hadler, K., Martin, D., Carpenter, J., Cilliers, J., Morse, A., Starr, S., Rasera, J., Seweryn, K., Reiss, P., Meurisse, A., 2020. A universal framework for space resource utilisation (sru). Planet. Space Sci. 182, 104811.

Ireland, P.M., 2010a. Triboelectrification of particulate flows on surfaces: Part i—experiments. Powder Technol. 198, 189–198.

Ireland, P.M., 2010b. Triboelectrification of particulate flows on surfaces: Part ii—mechanisms and models. Powder Technol. 198, 199–210.

Ireland, P.M., 2012. Dynamic particle-surface tribocharging: the role of shape and contact mode. J. Electrost. 70, 524–531.

Ireland, P.M., Nicholson, K., 2011. Analysis and comparison of particle tribochargers. Miner. Eng. 24, 914–922.

Kelly, E., Spottiswood, D., 1989a. The theory of electrostatic separations: a review part i. fundamentals. Miner. Eng. 2, 33–46.

Kelly, E., Spottiswood, D., 1989b. The theory of electrostatic separations: a review part iii. the separation of particles. Miner. Eng. 2, 337–349.

Kelly, E., Spottiwood, D., 1989. The theory of electrostatic separations: a review part ii. particle charging. Miner. Eng. 2, 193–205.

H. King, n.d. URL: https://geology.com/minerals/plagioclase.shtml.

H. King, n.d.. URL: https://geology.com/minerals/pyroxene.shtml.

H. King, n.d. URL: https://geology.com/minerals/olivine.shtml.

Kolehmainen, J., Ozel, A., Boyce, C.M., Sundaresan, S., 2016. A hybrid approach to computing electrostatic forces in fluidized beds of charged particles. AIChE J. 62, 2282–2295.

Kolehmainen, J., Ozel, A., Boyce, C.M., Sundaresan, S., 2017a. Triboelectric charging of monodisperse particles in fluidized beds. AIChE J. 63, 1872–1891.

Kolehmainen, J., Sippola, P., Raitanen, O., Ozel, A., Boyce, C.M., Saarenrinne, P., Sundaresan, S., 2017b. Effect of humidity on triboelectric charging in a vertically vibrated granular bed: experiments and modeling. Chem. Eng. Sci. 173, 363–373.

Lacks, D.J., 2012. The unpredictability of electrostatic charging. Angew. Chem. Int. Ed. 51, 6822–6823.

Lacks, D.J., Levandovsky, A., 2007. Effect of particle size distribution on the polarity of triboelectric charging in granular insulator systems. J. Electrost. 65, 107–112.

Laurentie, J.-C., Traoré, P., Dragan, C., Dascalescu, L., 2010. Numerical modeling of triboelectric charging of granular materials in vibrated beds. In: 2010 IEEE Industry Applications Society Annual Meeting, IEEE, pp. 1–6.

Laurentie, J., Traoré, P., Dascalescu, L., 2013. Discrete element modeling of triboelectric charging of insulating materials in vibrated granular beds. J. Electrost. 71, 951–957.

Lawver, J.E., Dyrenforth, W.P., 1973. Electrostatic separation. In: Electrostatics and its Applications, Wiley New York, pp. 221–249.

Li, T., Ban, H., Hower, J., Stencel, J., Saito, K., 1999. Dry triboelectrostatic separation of mineral particles: a potential application in space exploration. J. Electrost. 47, 133–142.

Li, X., Gan, H., Mo, B., Wang, S., Tang, H., Wei, G., Zhao, Y.-Y.S., 2016. Indication of mineral work function in lunar dust electrostatic migration. In: Proceedings of 47th Lunar and Planetary Science Conference, LPSC.

Manouchehri, H.-R., Hanumantha Rao, K., Forssberg, K., 2000a. Review of electrical separation methods - part 1: fundamental aspects. Min. Metall. Explor. 17, 23–36.

Manouchehri, H.-R., Hanumantha Rao, K., Forssberg, K., 2000b. Review of electrical separation methods - part 2: practical considerations. Min. Metall. Explor. 17, 139–166.

Matsusaka, S., Ghadiri, M., Masuda, H., 2000. Electrification of an elastic sphere by repeated impacts on a metal plate. J. Phys. Appl. Phys. 33, 2311.

McKay, D.S., Carter, J.L., Boles, W.W., Allen, C.C., Allton, J.H., 1994. Jsc-1: a new lunar soil simulant. Eng. Construct. Oper. Space IV 2, 857–866.

Perko, H.A., Nelson, J.D., Sadeh, W.Z., 2001. Surface cleanliness effect on lunar soil shear strength. J. Geotech. Geoenviron. Eng. 127, 371–383.

Quinn, J.W., Captain, J.G., Weis, K., Santiago-Maldonado, E., Trigwell, S., 2012. Evaluation of tribocharged electrostatic beneficiation of lunar simulant in lunar gravity. J. Aero. Eng. 26, 37–42.
Rasera, J., Cilliers, J., Lamamy, J., Hadler, K., 2019. The beneficiation of lunar regolith using electrostatic separation for space resource utilisation. In: Proceedings of 70th International Astronautical Congress, IAF.
Rasera, J., Cilliers, J., Lamamy, J., Hadler, K., 2020. The beneficiation of lunar regolith for space resource utilisation: a review. Planet. Space Sci. 186, 104879.
Rasera, J.N., Cilliers, J.J., Lamamy, J.A., Hadler, K., 2023. A methodology for tribocharger design optimisation using the Discrete Element Method (DEM). Powder Technol. 413, 118035.
Rasera, J., Cruise, R., Cilliers, J., Lamamy, J.-A., Hadler, K., 2022. Modelling the tribocharging process in 2d and 3d. Powder Technol., 117607
Schein, L., LaHa, M., Novotny, D., 1992. Theory of insulator charging. Phys. Lett. 167, 79–83.
Schrader, C., Rickman, D., McLemore, C., Fikes, J., 2010. Lunar Regolith Simulant User's Guide. Technical Report.
Sippola, P., Kolehmainen, J., Ozel, A., Liu, X., Saarenrinne, P., Sundaresan, S., 2018. Experimental and numerical study of wall layer development in a tribocharged fluidized bed. J. Fluid Mech. 849, 860–884.
Trigwell, S., Grable, N., Yurteri, C.U., Sharma, R., Mazumder, M.K., 2003. Effects of surface properties on the tribocharging characteristics of polymer powder as applied to industrial processes. IEEE Trans. Ind. Appl. 39, 79–86.
Trigwell, S., Captain, J., Arens, E., Captain, J., Quinn, J., Calle, C., 2007. The use of tribocharging in the electrostatic beneficiation of lunar simulant. In: Physics Electrostatics 2007 Conference, KSC-2007-013.
Trigwell, S., Captain, J.G., Arens, E.E., Quinn, J.W., Calle, C.I., 2009. The use of tribocharging in the electrostatic beneficiation of lunar simulant. IEEE Trans. Ind. Appl. 45, 1060–1067.
Trigwell, S., Captain, J., Weis, K., Quinn, J., 2012. Electrostatic beneficiation of lunar regolith: applications in in situ resource utilization. J. Aero. Eng. 26, 30–36.
Waitukaitis, S.R., Lee, V., Pierson, J.M., Forman, S.L., Jaeger, H.M., 2014. Size-dependent same-material tribocharging in insulating grains. Phys. Rev. Lett. 112, 218001.
Wills, B.A., Finch, J., 2015. Wills' Mineral Processing Technology: an Introduction to the Practical Aspects of Ore Treatment and Mineral Recovery. Butterworth-Heinemann.
Wilson, R., 1966. Vacuum thermionic work functions of polycrystalline be, ti, cr, fe, ni, cu, pt, and type 304 stainless steel. J. Appl. Phys. 37, 2261–2267.
Yamada, I., Shoji, S., 1990. Heavy solution method for determination of volcanic glass content in tephras and tephra-derived soils. Soil Sci. Plant Nutr. 36, 505–509.
Yang, X., Wang, H., Peng, Z., Hao, J., Zhang, G., Xie, W., He, Y., 2018. Triboelectric properties of ilmenite and quartz minerals and investigation of triboelectric separation of ilmenite ore. Int. J. Min. Sci. Technol. 28, 223–230.
Zhao, H., Castle, G.P., Inculet, I.I., Bailey, A.G., 2003. Bipolar charging of poly-disperse polymer powders in fluidized beds. IEEE Trans. Ind. Appl. 39, 612–618.